


## Article

# Prediction of Biome-Specific Potential Evapotranspiration in Mongolia under a Scarcity of Weather Data

Khulan Batsukh <sup>1</sup>, Vitaly A. Zlotnik <sup>1</sup>, Andrew Suyker <sup>2</sup> and Paolo Nasta <sup>3,\*</sup> 

<sup>1</sup> Department of Earth and Atmospheric Sciences, University of Nebraska-Lincoln, Lincoln, NE 68588, USA; hulanbatsuh99@gmail.com (K.B.); vzlotnik1@unl.edu (V.A.Z.)

<sup>2</sup> School of Natural Resources, University of Nebraska-Lincoln, Lincoln, NE 68588, USA; asuyker1@unl.edu

<sup>3</sup> Department of Agricultural Sciences, University of Naples Federico II, 80055 Naples, Italy

\* Correspondence: paolo.nasta@unina.it; Tel.: +39-081-253-9012

**Abstract:** We propose practical guidelines to predict biome-specific potential evapotranspiration ( $ET_p$ ) from the knowledge of grass-reference evapotranspiration ( $ET_0$ ) and a crop coefficient ( $K_c$ ) in Mongolia. A paucity of land-based weather data hampers use of the Penman–Monteith equation (FAO-56 PM) based on the Food and Agriculture Organization (FAO) guidelines to predict daily  $ET_0$ . We found that the application of the Hargreaves equation provides  $ET_0$  estimates very similar to those from the FAO-56 PM approach. The  $K_c$  value is tabulated only for crops in the FAO-56 guidelines but is unavailable for steppe grasslands. Therefore, we proposed a new crop coefficient,  $K_{c\ adj}$  defined by (a) net solar radiation in the Gobi Desert ( $K_{c\ adjD}$ ) or (b) leaf area index in the steppe region ( $K_{c\ adjS}$ ) in Mongolia. The mean annual  $ET_p$  obtained using our approach was compared to that obtained by FAO-56 guidelines for forages (not steppe) based on tabulated  $K_c$  values in 41 locations in Mongolia. We found the differences are acceptable (RMSE of 0.40 mm d<sup>−1</sup>) in northern Mongolia under high vegetation cover but rather high (RMSE of 1.69 and 2.65 mm d<sup>−1</sup>) in central and southern Mongolia. The FAO aridity index (AI) is empirically related to the  $ET_p/ET_0$  ratio. Approximately 80% and 54% reduction of  $ET_0$  was reported in the Gobi Desert and in the steppe locations, respectively. Our proposed  $K_{c\ adj}$  can be further improved by considering local weather data and plant phenological characteristics.

**Keywords:** Gobi Desert; steppe grasslands; crop coefficient; solar radiation; arid climate; leaf area index



**Citation:** Batsukh, K.; Zlotnik, V.A.; Suyker, A.; Nasta, P. Prediction of Biome-Specific Potential Evapotranspiration in Mongolia under a Scarcity of Weather Data. *Water* **2021**, *13*, 2470. <https://doi.org/10.3390/w13182470>

Academic Editor: Junzeng Xu

Received: 6 July 2021

Accepted: 4 September 2021

Published: 8 September 2021

**Publisher's Note:** MDPI stays neutral with regard to jurisdictional claims in published maps and institutional affiliations.



**Copyright:** © 2021 by the authors. Licensee MDPI, Basel, Switzerland. This article is an open access article distributed under the terms and conditions of the Creative Commons Attribution (CC BY) license (<https://creativecommons.org/licenses/by/4.0/>).

## 1. Introduction

Groundwater represents a vital water resource for ecosystems within an arid continental climate. Management of this resource relies on the knowledge of groundwater recharge (GR). However, in vast territories such as Mongolia, direct measurements of GR are unrealistic because they involve excessive costs from time-consuming and labor-intensive efforts. The use of hydrological models for simulating the water balance (and GR) within the groundwater–soil–plant–atmosphere continuum represents a valid alternative to direct measurements if the soil hydraulic properties and vegetation characteristics are properly assessed and initial and boundary conditions are well-known [1]. The main advantage of modeling is that the user needs only crop-specific potential evapotranspiration ( $ET_p$ ) and precipitation ( $P$ ) for obtaining simulations of GR. Precipitation measurements are commonly available and reasonably accurate. In contrast, obtaining a reliable prediction of  $ET_p$  represents a challenge in countries with limited availability of land-based, full suite weather data. This  $ET_p$  may be estimated by multiplying a grass-reference crop evapotranspiration ( $ET_0$ ) by a time-variant crop coefficient,  $K_c$  [2]. The reference grass is defined as a hypothetical crop with a height of 0.12 m, a surface resistance of 70 s m<sup>−1</sup>, and an albedo of 0.23 in a well-watered field [2]. Subsequently,  $ET_p$  is partitioned into potential evaporation

( $E_p$ ) and potential transpiration ( $T_p$ ) depending on the knowledge of leaf area index ( $LAI$ ) or vegetation cover fraction.

The concept of potential evapotranspiration is broadly used in hydrology and supported by established methods and software packages that account for non “well-watered” soil moisture conditions (e.g., HYDRUS [3] and MODFLOW [4]). The  $E_p$  and  $P$  represent the system-dependent boundary conditions of the hydrologic model over the soil profile, while  $T_p$  refers to potential root water uptake. Therefore, a reliable prediction of  $ET_p$  is fundamental in numerical models for obtaining the GR and actual evapotranspiration ( $ET_a$ ) that represents a reduction of  $ET_p$  induced by water stress.

The available models to estimate  $ET_0$  can be classified as: (i) full physically based models describing mass and energy conservation principles; (ii) semi-physically based models that deal with either mass or energy conservation; and (iii) black-box models based on empirical relationships and machine learning algorithms [5–7]. The Penman–Monteith equation, based on the Food and Agriculture Organization (FAO) guidelines (FAO-56 PM), is internationally recognized as the standard approach for computing  $ET_0$  [2,8]. This equation is considered the most reliable method as it is based on the energy balance incorporating physiological and aerodynamic parameters without any local calibration under all types of climatic conditions [2,9]. However, the FAO-56 PM method entails the availability of a complete, continuous suite of weather data including solar radiation, wind speed, air temperature, and relative humidity. However, these variables are often unavailable in data-limited countries where meteorological parameters are hard to obtain or are available only in the form of useless short-time series that differ among stations by periods of data collection. Some countries do not have a uniform distribution of full-suite weather sites or lack public access to these data, hindering large-scale and long-term agro-hydrological studies. However, long-term air temperature data are primarily available in spatially dense weather networks across Mongolia.

Daily  $ET_0$  is converted into biome-specific potential evapotranspiration ( $ET_p$ ), which refers to the evapotranspiration demand from a grassland biome (e.g., steppe grassland in Mongolia) under optimum soil water conditions [10]. This conversion entails the knowledge of the time-variant crop coefficient,  $K_c$ , which is well-documented for vegetables, cereals, forages, and fruit trees [2]. However, to our knowledge, a  $K_c$  representing vegetation properties under natural vegetation conditions in Mongolia is currently unavailable in the body of literature [11–13]. Obtaining this coefficient will allow one to estimate  $ET_p$  at daily time steps. This approach is more efficient than inferring values from images of remote sensing data only as noted by [14], who studied  $ET_0$  from the north China regions bordering with Mongolia.

According to [15], the normalized difference vegetation index (NDVI) shows strong positive correlations with evapotranspiration over the majority of grassland areas except for the region near the Gobi Desert [16]. Significant difference occurs between  $ET_0$  and  $ET_a$  in this biome. Hence, the regular  $K_c$  taken from FAO guidelines is not appropriate in the arid, sparsely vegetated Gobi Desert areas. Research from Inner Mongolia (China) supports this assumption [13]. Therefore, one may adapt a time-variant crop coefficient,  $K_{c\ adj}$  to steppe grasslands in Mongolia depending on satellite-derived leaf area index ( $LAI$ ) in the steppe region ( $K_{c\ adjS}$ ) and solar net radiation in the Gobi Desert ( $K_{c\ adjD}$ ). Net solar radiation can be estimated from easily accessible weather data, while monthly maps of leaf area index can be retrieved from remote sensing products.

To address this  $ET_p$  knowledge gap in Mongolia, we propose a two-fold approach. The first objective is to select a suitable temperature method to estimate daily  $ET_0$  values under data paucity constraints. A limited number of sites with full-suite weather data may be used to evaluate estimates of  $ET_0$ . The second objective is to develop a new time-variant crop coefficient ( $K_{c\ adj}$ ) to convert  $ET_0$  into  $ET_p$  in Mongolian biomes. The mean annual  $ET_p$  obtained using this approach could be compared to that obtained by FAO-56 guidelines for forages (not steppe) based on tabulated  $K_c$  values in locations across Mongolia.

Ultimately, these estimates of  $ET_p$  will be used as crucial input data for ground water recharge models which will be presented in future work.

## 2. Materials and Methods

### 2.1. Environmental Settings and Data Availability

Mongolia is a landlocked territory covering about 1.6 million km<sup>2</sup>, located in the heart of the Asian continent. Mongolia has borders with the Russian Federation in the north (3543 km long) and China in the south (4709 km) [17]. Mongolia lies on a high plateau surrounded by mountain ridges in the transition zone between the Siberian taiga and the dry steppes and semi-deserts of central Asia. The country has a dry subarctic continental climate with long cold winters and short hot summers.

The average number of rainy days per year is 105–115. Annual average precipitation ( $P$ ) is generally low decreasing from the north (350–500 mm) to the south (less than 50 mm) [17]. Maximum (almost 85%) seasonal  $P$  occurs in summer [8]. The average annual temperature ranges from  $-8\text{ }^{\circ}\text{C}$  to  $+2\text{ }^{\circ}\text{C}$  and is negative from October to March in most parts of the country [17].

In this territory, 80% is pasture-land, 10% forest, 1% farmland, and 9% other types of land. Steppe vegetation is the most common in Mongolia and occupies about 83% of the territory [18]. It lies mainly in the central part of the country, the transitional zone bordering the Gobi Desert to the south, and mountain taiga to the north. The steppe ecosystems are associated with the semi-arid and arid continental temperate climates of the region and are ecologically fragile and sensitive to climate change and anthropogenic disturbances [19]. Perennial plants (50–90%) dominate the Mongolian steppe. The highest percentage of perennial plants occurs in the high-cold steppe. In contrast, the percentage of shrub, dwarf shrub, biennials, and annuals is minimum in the high-cold steppe and gradually increases in the desert steppe [18]. About half of the Mongolian territory is mountainous with an average elevation of 1580 m a.s.l.; about 81% of its territory is above 1000 m and 19% below 1000 m [17]. These mountains are divided into cool and dry types according to their formation of vertical vegetation range. Khentii, Khuvsgul, northwestern Mongolian Altai, Northern Khangai, and Khyangan are referred to as cool type mountains and comprise steppe vegetation. Southern Altai, Gobi Altai, Gobi, and Zuungar mountains are referred to as dry type with desert vegetation and high-cold steppe [18].

We identified a total of 41 locations relatively uniformly distributed across Mongolia with available weather data (Figure 1). We specified that ten weather stations (blue triangles in Figure 1) had a complete set of weather data, while the remaining 31 stations (black triangles) provided only  $T$  and  $P$  data. The study locations were chosen considering the density, physical geography, latitude and altitude, land use, climate class, and data availability.

The complete data set belonging to the ten weather stations will be exploited for estimating daily  $ET_0$  with the FAO-56 PM equation and temperature-based equations (Section 2.2.). Table 1 shows information on data sources used in this study for all 41 study locations.

**Table 1.** Information (time-period, location, and reference) of data sources.

Collected Data/Parameters	Unit	Period of Data Availability	Source	References
Daily $P$	mm	2007–2011	NAMEM	[21]
Daily max $T$ , min $T$ , mean $T$	( $^{\circ}\text{C}$ )	2001–2020	NOAA National Centers for Environmental Information	[22]
$LAI$	(-)	1981–2015	ORNL DAAC	[23]

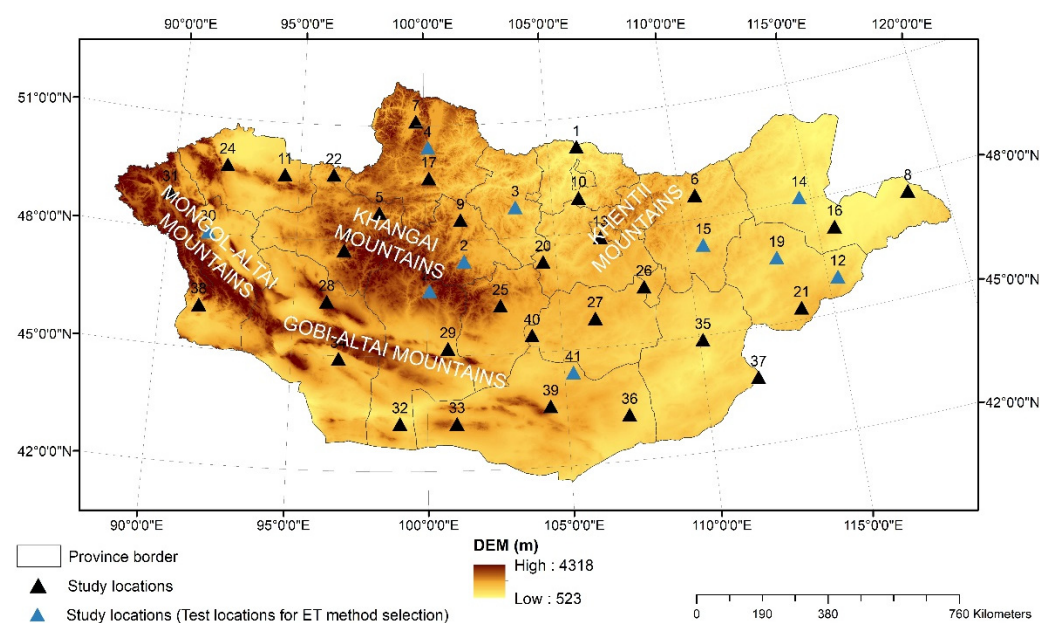


**Figure 1.** Locations of 41 weather stations (represented by the triangle symbol) on the digital elevation model (DEM) retrieved from the Shuttle Radar Topography Mission (SRTM) in Mongolia [20]. The ten blue triangles indicate the weather stations with a complete set of meteorological data used to compare FAO-56 PM with temperature-based equations.

Daily  $P$  data were retrieved from the National Agency of Meteorology and Environmental Monitoring (NAMEM) [21].  $T$  data at Khatgal weather station were validated with those obtained from the National Oceanic and Atmospheric Administration (NOAA) website [22]. This comparison shows high correlation between remote-sensing and ground-truthing data (available in Figure S1 in Supplemental Materials). Since the ground-based leaf area index ( $LAI$ ) measurements are highly variable in space and time, the estimates from the remotely sensed products were assumed valid and reliable and were not validated with ground-truth measurements [24]. The  $LAI$  monthly mean values were obtained from the Oak Ridge National Laboratory Distributed Active Archive Center (ORNL DAAC) website [23] providing a global  $0.25^\circ \times 0.25^\circ$  gridded monthly mean  $LAI$  over the period from August 1981 to August 2015. The data were derived from the Advanced Very High-Resolution Radiometer (AVHRR) Global Inventory Modeling and Mapping Studies (GIMMS), and the bi-weekly  $LAI$  values were averaged for every month (Figure S2 in Supplemental Materials). Due to the low vegetation cover, the  $LAI$  in some parts of the Gobi Desert is unavailable. The inverse distance weighted interpolation tool was used in ArcGIS software (Esri, West Redlands, CA, USA) to estimate the weighted average of the  $LAI$  values in the neighborhood of each processing cell. As it follows from the name, this method uses the inverse distance to each point when assigning weights. The monthly average values of  $LAI$  extracted from the map at study locations are available (Figure S3 in Supplemental Materials).

## 2.2. Prediction of Reference Evapotranspiration, $ET_0$ , and Biome-Specific Potential Evapotranspiration, $ET_p$

We considered two well-known limited-data-requirement equations to predict  $ET_0$ , namely, Hargreaves (Har) [25] and Thornthwaite (Tho) [26,27]. We evaluated the prediction performance of Har and Tho equations by comparing these two methods with the FAO-56 PM equation by using a complete meteorological dataset at 10 weather stations [28–30] and selected the best performing temperature method to estimate  $ET_0$  (Figure 2a).

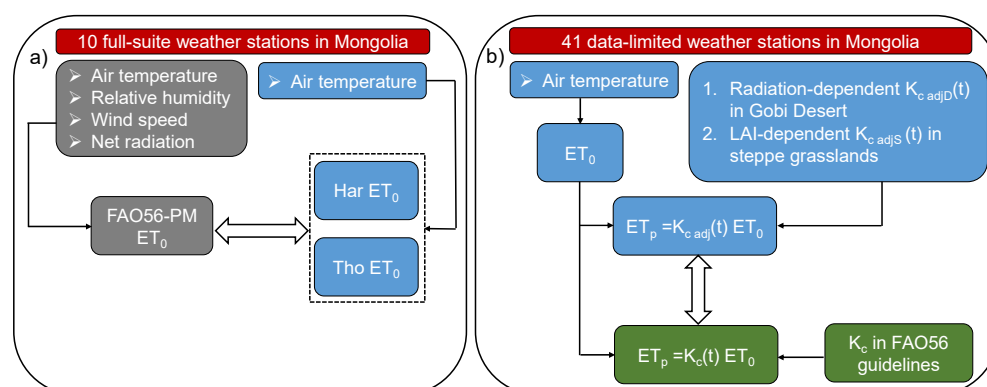


**Figure 2.** Schematic overview for estimating (a) grass-reference potential evapotranspiration,  $ET_0$  derived from FAO-56 PM (gray boxes) and temperature-based equations, Har and Tho (blue boxes), using data from 10 weather stations (garnet boxes); and (b) biome-specific potential evapotranspiration,  $ET_p$ , derived from  $K_c$  tabulated in the FAO-56 guidelines (green boxes) and from a new  $K_{c adj}$  (blue boxes) using data from 41 weather stations (garnet boxes). The new crop coefficient,  $K_{c adj}$  depends on net solar radiation in the Gobi Desert ( $K_{c adjD}$ ) or (b) leaf area index in the steppe region ( $K_{c adjS}$ ).

The equations are reported in Table 2, and we briefly report necessary input data for each equation. In the FAO-56 PM equation,  $R_n$  is net radiation at plant surface ( $\text{MJ m}^{-2} \text{d}^{-1}$ ),  $G$  is the soil heat flux density ( $\text{MJ m}^{-2} \text{d}^{-1}$ ),  $T$  is air temperature ( $^{\circ}\text{C}$ ),  $u_2$  is the wind speed at 2 m height above ground ( $\text{m s}^{-1}$ ),  $e_s$  and  $e_a$  are saturated and actual vapor pressures (kPa),  $\Delta$  is the slope of the vapor pressure curve ( $\text{kPa } ^{\circ}\text{C}^{-1}$ ), and  $\gamma$  is the psychrometric constant ( $\text{kPa } ^{\circ}\text{C}^{-1}$ ). Net radiation is usually indirectly measured by a pyranometer. If a weather station lacks pyranometer data,  $R_n$  can be estimated from the actual daily duration of bright sunshine (hours per day) [2]. The term  $G$  is computed as a fraction of  $R_n$ , as suggested by [2] for the reference crop. In the Har equation,  $R_a$  is the extraterrestrial radiation expressed in  $\text{mm d}^{-1}$  (obtained by multiplying  $\text{MJ m}^{-2} \text{d}^{-1}$  by 0.408),  $T_m$  ( $^{\circ}\text{C}$ ),  $T_{min}$  ( $^{\circ}\text{C}$ ), and  $T_{max}$  ( $^{\circ}\text{C}$ ) represent mean, minimum, and maximum temperature, respectively. In the Tho equation, the value  $I$  represents the annual heat index,  $T_m$  represents  $i$ -th month mean air temperature ( $^{\circ}\text{C}$ ), and  $h$  depicts hours of sunlight (hours).

**Table 2.** FAO-56 PM, Har and Tho equations with required input data to calculate daily  $ET_0$ .

The Methods	Minimum Meteorological Data Requirements						Equations
	Mean $T$	Max $T$	Min $T$	Relative Humidity	Wind Speed	$R_a$ or $R_n$	
FAO-56 PM	+	+	+	+	+	+	$ET_0 = \frac{0.408\Delta(R_n - G) + \gamma \frac{900}{T + 273} u_2 (e_s - e_a)}{\Delta + \gamma(1 + 0.34u_2)}$
Hargreaves	+	+	+			+	$ET_0 = 0.0023(T_m + 17.8)(T_{max} - T_{min})^{0.5}(0.408R_a)$
Thornthwaite modified	+						$ET_0 = \begin{cases} 0, & T < 0^{\circ} \\ 0.553 \left( \frac{10T}{T + 17.8} \right)^a, & 0 \leq T \leq 26.5^{\circ} \\ (-13.86 + 1.075T - 0.0144T^2) \frac{h}{12}, & T \geq 26.5^{\circ} \end{cases}$ $I = \sum_{i=1}^{12} \left( \frac{T_m}{5} \right)^{1.514}$ $\alpha = (6.75 \times 10^{-7} I^3) - (7.71 \times 10^{-5} I^2) + (1.79 \times 10^{-2} I) + 0.492$

The daily maximum, minimum, mean temperature, relative humidity, and wind speed data were obtained from NAMEM [21]. The hours of sunlight data were downloaded at the nearest available station [31]. The terms  $R_a$  and  $R_n$  were indirectly estimated from the guidelines on missing climatic data from the FAO-56 report [2].



The FAO-based aridity index ( $AI$ ) is computed as the ratio between mean annual  $P$  and  $ET_0$  [32] and will be used in our study. This index can be considered a proper indicator for climate classification in Mongolia.

After selecting the best temperature model, daily  $ET_0$  was calculated in all 41 study locations with easily accessible data. The crop coefficient considers plant characteristics, such as height, leaf area index, and leaf and stomata properties in order to convert the reference grass  $ET_0$  into  $ET_p$ . These plant characteristics indeed influence the aerodynamic resistance, the albedo of crop-soil surface, and canopy resistance. The FAO-56 guidelines report [2] tabulated  $K_c$  values for crops, vegetables, forages, and fruit trees referring to a sub-humid climate with an average daytime minimum relative humidity of about 45% and with wind speeds averaging  $2 \text{ m s}^{-1}$ . These tabulated  $K_c$  values under the abovementioned climatic conditions are not present in Mongolia. A study carried out in neighboring parts of Inner Mongolia [12] across the border demonstrates that a developed  $K_c$  for steppe in the arid and semi-arid zone is lower than the available  $K_c$  value (grazing pasture) taken from the FAO-56 guidelines [2]. The natural vegetation conditions in those climate zones have not been studied in-depth, unlike agricultural crops. Permanent monitoring stations are absent, and the exact vegetation condition in those arid, semi-arid areas is mostly unknown. Therefore, the use of guidelines to develop  $K_c$  from FAO-56 report [2] is fraught with uncertainties.

Nevertheless, the natural zones can be grouped into land cover zones of the Gobi Desert and the steppe (Table A1 in Appendix A). Then, different methods to develop  $K_c$  based on different climate and phenological characteristics for those two zones were explored and implemented in our study (Figure 2b). Previous studies have indicated that the  $K_c$  values vary significantly during the growing season; therefore, it is impossible to assume  $K_c$  as constant over time. This study attempts to propose a time-variant crop coefficient,  $K_{c,adj}$ , using easily-retrievable data, such as solar radiation or  $LAI$ , and therefore,  $ET_p$  values can be obtained ( $ET_p = ET_0 \times K_{c,adj}$ ) in study locations.

In the Gobi Desert ecosystem, the crop coefficient taken from the FAO-56 guidelines [2] is not suitable due to scarce and sparse vegetation. The following simple relation is, therefore, used to estimate daily variations of the proposed crop coefficient [12],  $K_{c,adjD}$ , based on the measurement of solar radiation:

$$K_{c,adjD} = 0.02 * R_n \quad (1)$$

where  $R_n$  is net solar radiation.

In the steppe zone in Mongolia, similar studies are scarce, and there are no readily available approaches providing crop coefficients in the FAO-56 report [2]. Some guidelines for (non-crop) grassland in arid climates require parameters such as vegetation height, air relative humidity, and wind speed, and their use is not straightforward. For example, the crop coefficient,  $K_{c,p}$ , in a non-irrigated pasture site in Florida, USA [33] ranged from 0.47 to 0.92 and could be presented by a linear function of leaf area index ( $LAI$ ):

$$K_{c,p} = aLAI + b \quad (2)$$

where the empirical parameters are assumed as  $a = 0.330$  and  $b = 0.451$ . However, the natural vegetation growth is subject to various constraints. Therefore, we propose to adapt the crop coefficient to steppe grassland ( $K_{c,adjS}$ ) proposed by [2] for sparse vegetation under local conditions:

$$K_{c,adjS} = K_{c,p} - A_{cm} \quad (3)$$

where  $A_{cm}$  is another empirical parameter given by the following equation:

$$A_{cm} = 1 - \left[ \frac{LAI}{LAI_{dense}} \right]^{0.5} \quad (4)$$

where  $LAI_{dense}$  is the  $LAI$  expected for the same crop under normal, standard crop management practices. The  $LAI_{dense}$  can be predicted from the ground cover ratio.

The same linear function could not be applied in all study locations throughout the steppe due to contrasting vegetation characteristics. After multiple attempts, the  $LAI_{dense}$  values in the steppe zone in study locations with higher-than-average  $LAI$  values ( $LAI > 0.6$ ) and locations with lower-than-average values ( $LAI < 0.6$ ) were calculated using the following equations:

$$LAI_{dense} = \begin{cases} \frac{0.95 - 0.2}{0.6 - 0} LAI + 0.2, & LAI < 0.6 \\ \frac{3.03 - 0.95}{2.53 - 0.6} (LAI - 0.6) + 0.95, & LAI > 0.6 \end{cases} \quad (5)$$

Figure 3 shows  $A_{cm}$  and  $LAI_{dense}$  as a function of  $LAI$ .

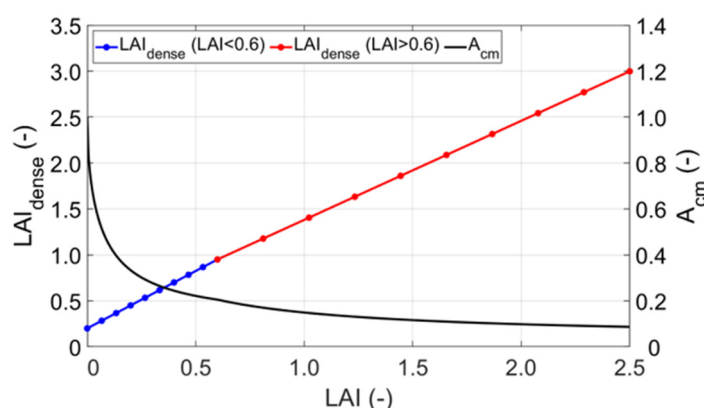


Figure 3.  $LAI_{dense}$  and  $A_{cm}$  values depending on  $LAI$ .

By estimating  $LAI_{dense}$  from Equation (5), daily  $K_{c\ adjs}$  and  $A_{cm}$  can be calculated in Equations (3) and (4), respectively, and therefore,  $ET_p$  values can be obtained ( $ET_0 \times K_{c\ adjs}$ ) in study locations belonging to the steppe zone in Mongolia. Grass pasture is assumed to be predominant in the steppe. The growing season of grass pasture is assumed to start seven days before recording 4 °C in spring for the last time until seven days after recording −4 °C in fall for the first time in all study locations. The crop coefficient in the dormant season is considered as 0.1 in all study locations by the guidance of [2].

As indicated above, leaf area index  $LAI$  plays a critical role in generating input data for modeling the water balance of the vadose zone. This parameter is used in Beer's law, which partitions  $ET_p$  into potential evaporation,  $E_p$ , and potential transpiration,  $T_p$  [34]:

$$E_p = ET_p e^{-kLAI} = ET_p (1 - SCF) = ET_p e^{-0.463LAI} \quad (6)$$

$$T_p = ET_p (1 - e^{-kLAI}) = ET_p SCF = ET_p - E_p \quad (7)$$

where  $SCF$  is the soil cover fraction (-), and  $k$  is the radiation extinction constant (-), usually assumed to be equal to 0.463 as indicated by various studies, e.g., [34–36].

### 2.3. Evaluation Criteria

To measure the predictive capability of all prediction methods mentioned above, we selected two statistical performance indicators: the root mean square error ( $RMSE$ ), which combines both bias and lack of precision, and the coefficient of determination ( $R^2$ ), which measures how well the data pairs fit to a line:

$$RMSE = \sqrt{\frac{1}{n} \sum_{i=1}^n (o_i - e_i)^2} \quad (8)$$

$$R^2 = \frac{\sum_{i=1}^n (o_i - e_i)^2}{\sum_{i=1}^n (o_i - \bar{o})^2} \quad (9)$$

where  $o_i$  is the reference value (for example, FAO-56 PM  $ET_0$ ),  $\bar{o}$  is the mean of reference values, and  $e_i$  indicates estimated values (for example,  $ET_0$ -Har and  $ET_0$ -Tho). Subscript  $i$  is the index of data in series (or day number), and  $n$  is the total number of days. Daily values of  $ET_0$  and  $ET_p$  will also be aggregated at monthly and annual sums; therefore, RMSE units are also expressed as mm month<sup>-1</sup> and mm year<sup>-1</sup>, respectively.

### 3. Results

#### 3.1. Prediction of Grass-Reference Evapotranspiration, $ET_0$

The relationship between meteorological variables and FAO-56 PM daily  $ET_0$  for 10 weather stations is expressed in terms of Pearson correlation coefficients presented in Table 3.

**Table 3.** Pearson correlation coefficients between FAO-56 PM daily  $ET_0$  and meteorological variables over the 10 weather stations in Mongolia.

	Wind Speed	Relative Humidity	Air Temperature	Net Radiation	Sunshine Hours
1. Galuut	0.51	−0.57	0.91	0.92	0.74
2. Tsetserleg	0.16	−0.23	0.91	0.91	0.84
3. Bulgan	0.30	−0.47	0.90	0.92	0.75
4. Khovd	0.58	−0.76	0.90	0.92	0.84
5. Erdenetsagaan	−0.02	−0.63	0.91	0.88	0.69
6. Choibalsan	0.04	−0.69	0.91	0.91	0.83
7. Khatgal	0.01	−0.28	0.90	0.92	0.85
8. Baruunurt	0.20	−0.72	0.91	0.90	0.71
9. Undurkhaan	0.20	−0.73	0.90	0.90	0.72
10. Tsogtovoo	0.21	−0.68	0.91	0.91	0.84

High positive correlation coefficients are observed between  $ET_0$  and air temperature and net radiation, while negative correlation coefficients are reported when relating  $ET_0$  to the relative humidity. The results agree with the conclusion of [37] that the net radiation and air temperature are the most important controlling factors on  $ET_0$ . This proves the potential of temperature-based  $ET_0$  models in Mongolia.

When considering estimates of daily  $ET_0$  values, the comparison between Har and FAO-56 PM equations (blue line in Figure 4) leads to a minimum RMSE of 0.56 mm d<sup>-1</sup> ( $R^2 = 0.93$ ) in Khatgal and a maximum RMSE of 1.44 mm d<sup>-1</sup> ( $R^2 = 0.87$ ) in Tsogtovoo. The comparison between Tho and FAO-56 PM equations (red line in Figure 4) spans between RMSE of 0.76 mm d<sup>-1</sup> ( $R^2 = 0.88$ ) in Bulgan and RMSE of 1.74 mm d<sup>-1</sup> ( $R^2 = 0.85$ ) in Tsogtovoo. The Har  $ET_0$  method shows lower RMSE and higher  $R^2$  than those obtained from the Tho equation over the 10 test locations. The comparison between FAO-56 PM-based and temperature-based equations for predicting daily values of  $ET_0$  at Khatgal and Tsogtovoo weather stations are presented in Figure S4 in Supplemental Materials.

A temperature-based model ignores the importance of meteorological variables such as relative humidity, solar radiation, and vapor pressure deficit, as diagnosed by high correlation coefficients listed in Table 3. The FAO-56 PM-based monthly cumulative  $ET_0$  also better matches with the Har method, as can be seen in Figure S5 in Supplemental Materials. One of the drawbacks of the Tho method is that  $ET_0$  can not be calculated in the winter months when the temperature drops below 0 °C. Therefore, according to the cumulative results, the Tho method systematically underestimates the reference  $ET_0$  estimated by the FAO-56 PM equation.



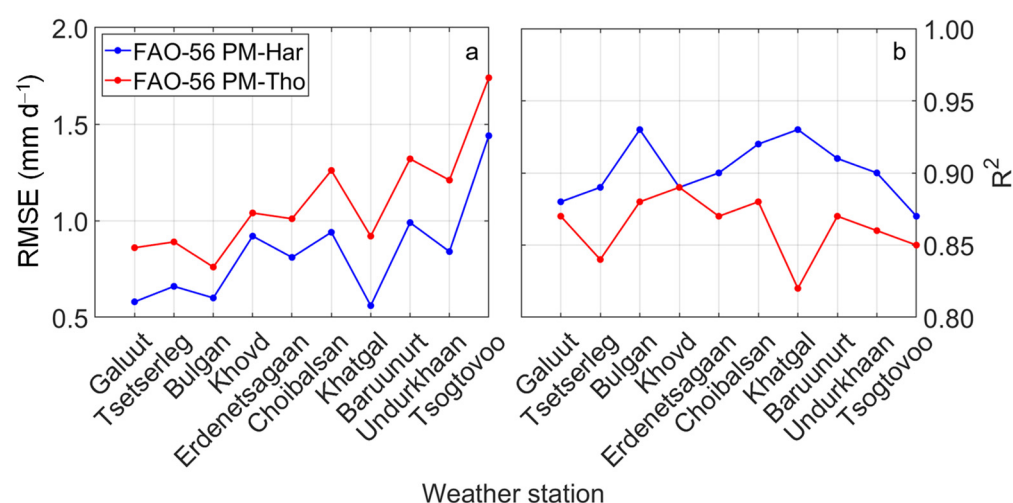


**Figure 4.** Model performance indicators comparing the FAO-56 PM with Har (blue line) and Tho (red line) to estimate daily values of  $ET_0$ : (a) RMSE (mm d<sup>-1</sup>) values and (b) values of  $R^2$  (-) for 10 weather stations.

The mean annual  $ET_0$  sums predicted by the three methods are visualized in Figure 5. The FAO-56 PM-based predictions of mean annual  $ET_0$  sums are in accordance with the estimates in Inner Mongolia (China) reported by [38].  $ET_0$ , predicted by the Har and Tho equations, consistently suffers from underestimation. RMSE is 159.3 mm y<sup>-1</sup> and 248.3 mm y<sup>-1</sup> for Har and Tho equation, respectively.

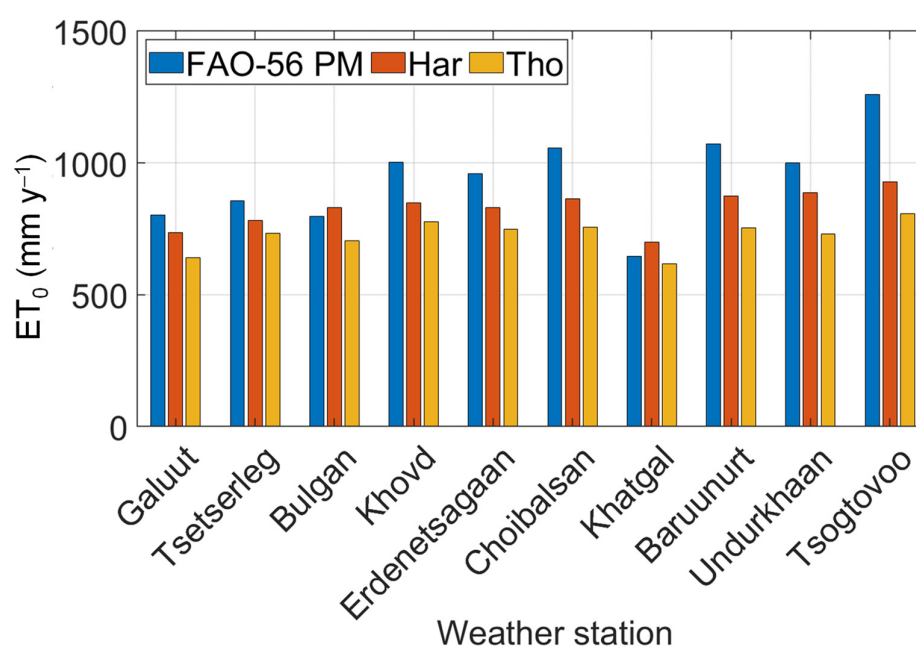


**Figure 5.** Mean annual grass-reference evapotranspiration,  $ET_0$  calculated with FAO-56 PM (blue bars), Har (orange bars), and Tho (yellow bars) for 10 weather stations in Mongolia.

As seen from the statistical results and cumulative comparisons, the Har outperforms the Tho equation for estimating  $ET_0$ . We concur with [39] that lack of local calibration might be unacceptable for practical applications. We are also aware that [40] observed that the Har equation generates a significant bias in northeastern China. However, we are forced to use the uncalibrated Har  $ET_0$  method due to the chronic data paucity in Mongolia. Therefore, we selected the Har equation over the 41 study locations to predict  $ET_0$ , which will be converted into  $ET_p$  in Section 3.2. Annual sums of Har- $ET_0$  are presented in Table A2

in Appendix A. The  $ET_0$  annual sums broadly varied in space with low temporal variability in each station through 5 years (2007–2011). The coefficient of variation (CV) was lower than 10% in 40 out of 41 stations. If we consider the spatial-average  $ET_0$  in each year, 2007 and 2011 had the highest and lowest values, respectively.

Finally, we carried out a second validation of the Har  $ET_0$  predictions. A global map of monthly  $ET_0$  estimated with FAO-56 PM referring to the period 1961–1990 [41] was used to aggregate the mean annual  $ET_0$  (Figure 6) and extract corresponding values over the 41 weather stations.

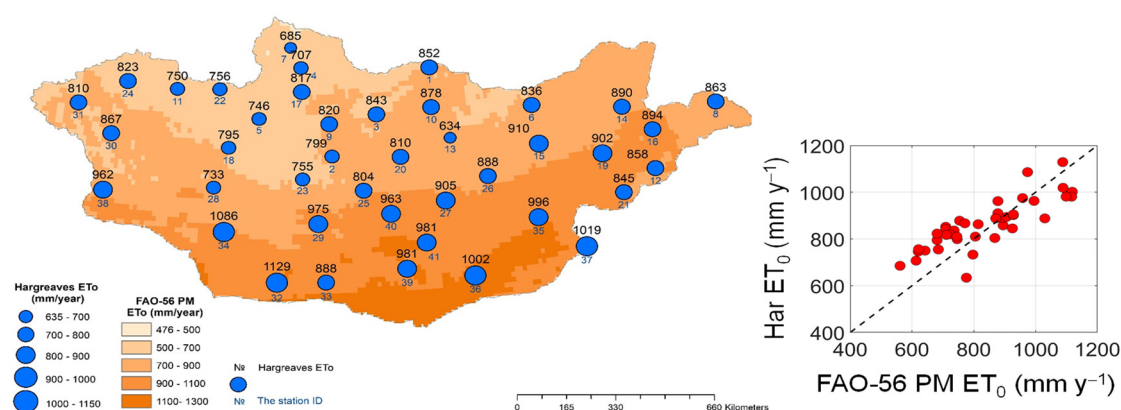


**Figure 6.** Map of mean annual FAO-56 PM  $ET_0$  estimated by FAO (2009) with corresponding Har  $ET_0$  values (blue circles). Plot on the right shows the comparison between FAO-56 PM  $ET_0$  and Har  $ET_0$ . Diagonal dashed line depicts the identity line (1:1 line).

$ET_0$  values tend to increase towards the south in general. The lowest mean annual  $ET_0$  value is 634 mm, while the highest is 1129 mm. The Har  $ET_0$  values are compared to the corresponding FAO-56 PM  $ET_0$  by obtaining  $RMSE = 93 \text{ mm y}^{-1}$  and  $R^2 = 0.69$ . Nevertheless, the Har-based  $ET_0$  results look consistent with [41] and previous studies carried out in Mongolia [8,25,42] and Inner Mongolia [14] and appear to form a reliable basis for further processing and modeling.

### 3.2. Prediction of Biome-Specific Potential Evapotranspiration, $ET_p$

The  $ET_p$  is calculated by multiplying  $ET_0$  with the time-variant  $K_{c \text{ adj}}$  in the Gobi Desert ( $K_{c \text{ adjD}}$ ) and in the steppe grasslands ( $K_{c \text{ adjS}}$ ), as described beforehand. By assuming the reliability of Har  $ET_0$  predictions, our attention is now focused on the assessment of crop coefficient,  $K_{c \text{ adj}}$  in Mongolia, and its impact on the prediction of  $ET_p$ . To this end, we considered six weather stations in the steppe region (Sukhbaatar, Tosontsengel, Baruunkharaa, Undurkhaan, Erdenesant, Arvaikheer) and one representative weather station in the Gobi Desert (Saikhanovoo) (Figure S6 in Supplemental Materials) where we predicted  $ET_p$  by using the developed  $K_{c \text{ adj}}$  for natural vegetation (Figure 7b) or the tabulated  $K_c$  (Figure S7 in Supplemental Material) based on grazing pasture in the FAO-56 guidelines (see Table 17 in [2]). Our developed crop coefficient,  $K_{c \text{ adj}}$ , depends on LAI (Figure 7a) retrieved from remote-sensing monthly maps in the grassland steppe ( $K_{c \text{ adjS}}$ ) or on solar radiation in the Gobi Desert ( $K_{c \text{ adjD}}$ ). We observed a decrease in LAI (Figure S2 in Supplemental Materials) and  $K_{c \text{ adjS}}$  towards the south, where conditions become arid. The use of time-variant LAI has the advantage of generating time-variant  $K_{c \text{ adjS}}$  according to our methodology. In contrast, tabulated values in the FAO-56 report provide constant  $K_c$  values in three growing season phases.

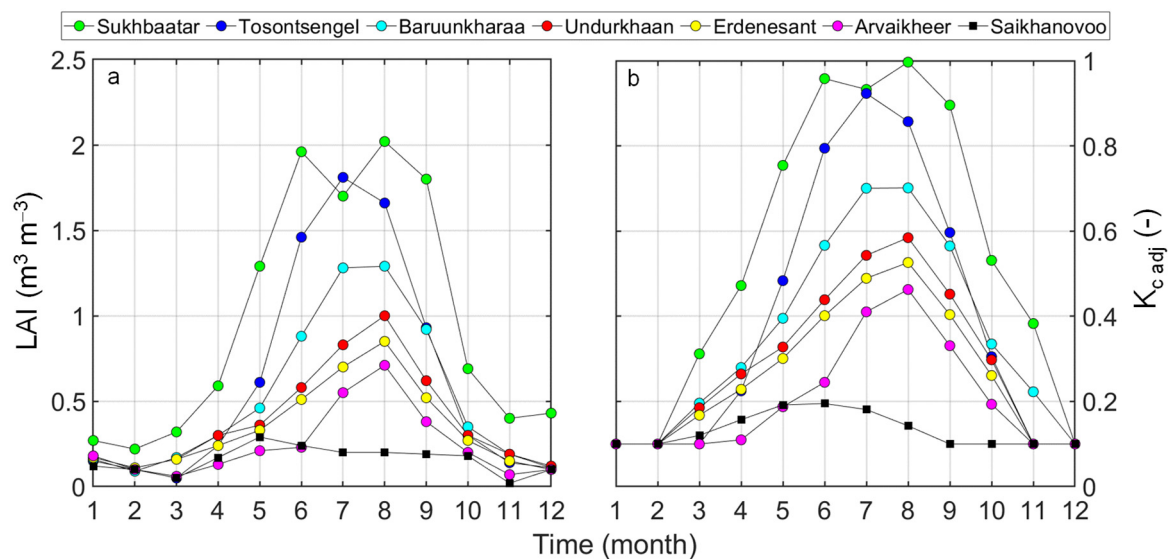


**Figure 7.** Mean monthly values of (a) leaf area index ( $LAI$ ) and (b) crop coefficient,  $K_{c\ adjS}$  at six weather stations (Sukhbaatar, Tosontsengel, Baruunkharaa, Undurkhaan, Erdenesant, Arvaikheer) in the steppe zone (colored circles) and crop coefficient,  $K_{c\ adjD}$  at one weather station (Saikhanovoo) in the Gobi Desert (black square).

The developed ( $K_{c\ adj}$ ) and tabulated  $K_c$  values are used to convert  $ET_0$  into biome-specific  $ET_p$ . Figure 8 shows an illustrative example by comparing predictions of  $ET_p$  at three stations (Sukhbaatar, Arvaikheer and Saikhanovoo) with contrasting vegetation cover.  $K_{c\ adjS}$  is used at Sukhbaatar and Arvaikheer (steppe region) while  $K_{c\ adjD}$  is used at Saikhanovoo (Gobi Desert). The prediction of  $ET_p$  with both  $K_{c\ adj}$  and tabulated  $K_c$  values was similar over the first weather station (Sukhbaatar), with vegetation cover characterized by  $LAI > 1$  and  $K_{c\ adjS} > 0.6$  during the growing season in summer (green circles in Figure 7). Nevertheless, vegetation cover halved at the second weather station (Arvaikheer) or reduced to almost zero at the third weather station in the Gobi Desert (Saikhanovoo) in terms of  $LAI$  and  $K_{c\ adj}$  (Figure 7). The impact of the developed  $K_{c\ adj}$  value on the  $ET_p$  prediction can be visualized in Figure 8. The tabulated  $K_c$  values (red circles in Figure 8a–c) generated similar predictions of  $ET_p$  over the three stations despite the contrast in vegetation cover. On the other hand, the impact of the scarce vegetation cover on the developed  $K_{c\ adj}$  value over Arvaikheer and especially Saikhanovoo in the Gobi Desert induced a drastic reduction in  $ET_p$  (blue circles in Figure 8a–c). The comparison between  $ET_p$  predictions based on tabulated  $K_c$  and  $ET_p$  predictions based on developed  $K_{c\ adj}$  is shown in Figure 8d–f. Despite high  $R^2$  values diagnosing similar temporal trends in response to seasonal temperature change, we report consistent bias over the weather station at Arvaikheer ( $RMSE = 1.69\text{ mm d}^{-1}$ , Figure 8e) and Saikhanovoo ( $RMSE = 2.65\text{ mm d}^{-1}$ , Figure 8f) in the Gobi Desert.

In contrast, both tabulated and developed  $K_{c\ adjS}$  at the weather station of Sukhbaatar led to a similar prediction of  $ET_p$  (Figure 8d) as diagnosed by a very low  $RMSE$  ( $RMSE = 0.40\text{ mm d}^{-1}$ ).

The mean annual sums of  $ET_p$  based on tabulated (orange bars) and developed (blue bars)  $K_c$  over the seven weather stations are displayed in Figure 9 with increasing discrepancy under scarce vegetation cover conditions, characterized by a gradient from north to south. Very low differences of 52.6 mm and 140.5 mm are shown at Sukhbaatar and Tosontsengel, respectively. The highest differences were reported in the following four stations with 298.8 mm, 385.2 mm, 365.7 mm, and 407.4 mm at Baruunkharaa, Undurkhaan, Erdenesant, and Arvaikheer, respectively. The highest difference of 674.3 mm was reported at Saikhanovoo in the Gobi Desert.

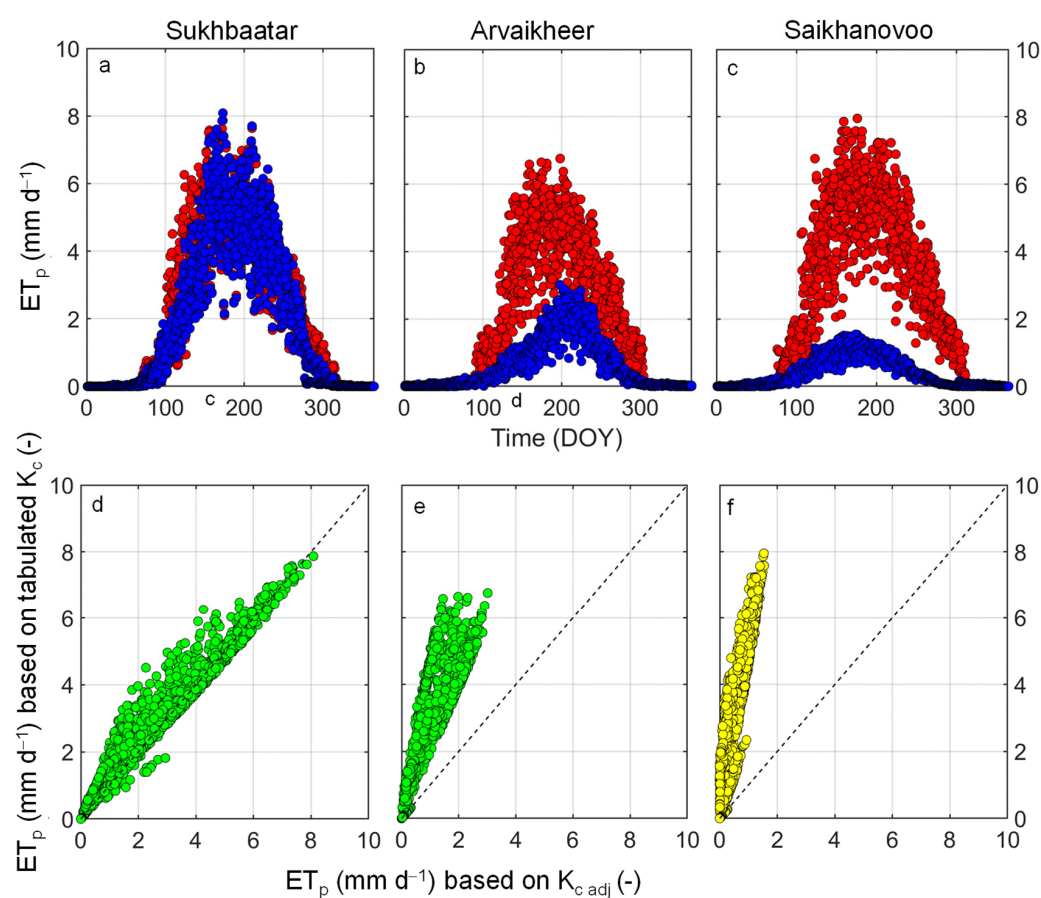


**Figure 8.** Comparison between daily  $ET_p$  values based on  $K_{c\ adj}$  (blue circles) and  $ET_p$  values based on tabulated  $K_c$  (red circles) over (a) Sukhbaatar, (b) Arvaikheer, and (c) Saikhanovoo. The data scatter (green and yellow circles distinguish steppe and Gobi Desert) around the identity line (1:1 line represented by the diagonal dashed line) is illustrated in (d) Sukhbaatar, (e) Arvaikheer, and (f) Saikhanovoo.

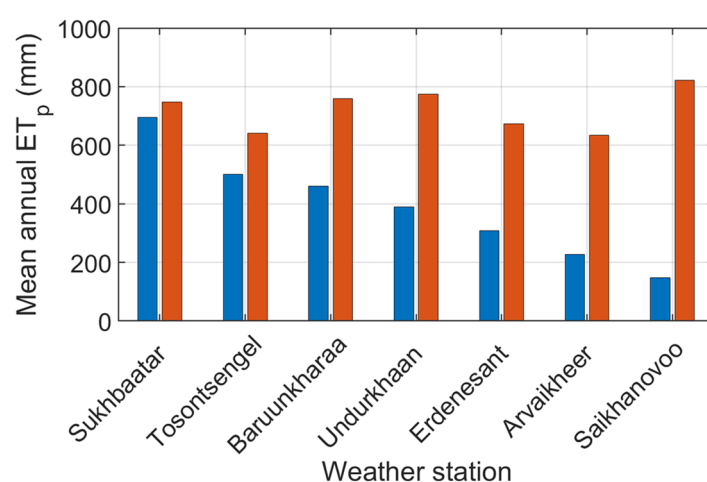


**Figure 9.** Mean annual sums of  $ET_p$  based on  $K_{c\ adj}$  (blue bars) and on tabulated  $K_c$  (orange bars) over six weather stations in Mongolia.

Mean annual sums of  $P$ ,  $ET_0$ ,  $ET_p$  (based on our developed  $K_c$ ),  $T_p$ , and  $E_p$  and corresponding aridity index,  $AI$ , over the 41 study locations in Mongolia are presented in Table A3 in Appendix A.

We observe the consistent reduction of  $ET_0$  into  $ET_p$  in accordance with the study presented by [13] in arid and semi-arid classes. The difference between  $ET_0$  and  $ET_p$  increases over the Gobi Desert region, where the  $K_{c\ adj}$  values decrease consistently.

The aridity increases to the south with mean annual temperature increase, and precipitation decrease (Figure S8 in Supplemental Materials). Therefore, the effect from mountain ranges also can be perceived, especially in the south part of Mongol-Altai and Gobi-Altai mountain ranges. The ratio of  $ET_0$  to  $P$  varies from 3 to 12 times in study locations, while the ratio  $ET_p$  to  $P$  is about 2.5 to 3 times.  $E_p$  constitutes a large portion of  $ET_p$  with low  $LAI$  in the southern Gobi Desert locations (Figure S9 in Supplemental Materials). In contrast, in northern Mongolia,  $T_p$  importance increases, as seen from Table A3. Especially in the Gobi Desert region,  $E_p$  constitutes more than 86% of  $ET_p$  over the study locations. The variations in  $T_p$  closely follow the variation in  $LAI$ . All study locations in Mongolia are categorized into the arid macro-class, and  $AI$  ranges from 0.05 to 0.40. According to Table A3, climate classes belong to arid to semi-arid classes in study locations.  $ET_0$  values are high in the Gobi Desert region due to the high mean temperatures. On the other hand, the  $ET_p$  values consistently decrease in the Gobi Desert Region due to very low  $LAI$  values characterizing scarce vegetation cover as depicted by very low daily  $K_{c\ adjD}$  values in the Gobi Desert in Figure 10a. The difference between mean annual  $ET_0$  and  $ET_p$  gets higher in the Gobi Desert and closer in the steppe (Figure S10 in Supplemental Materials).

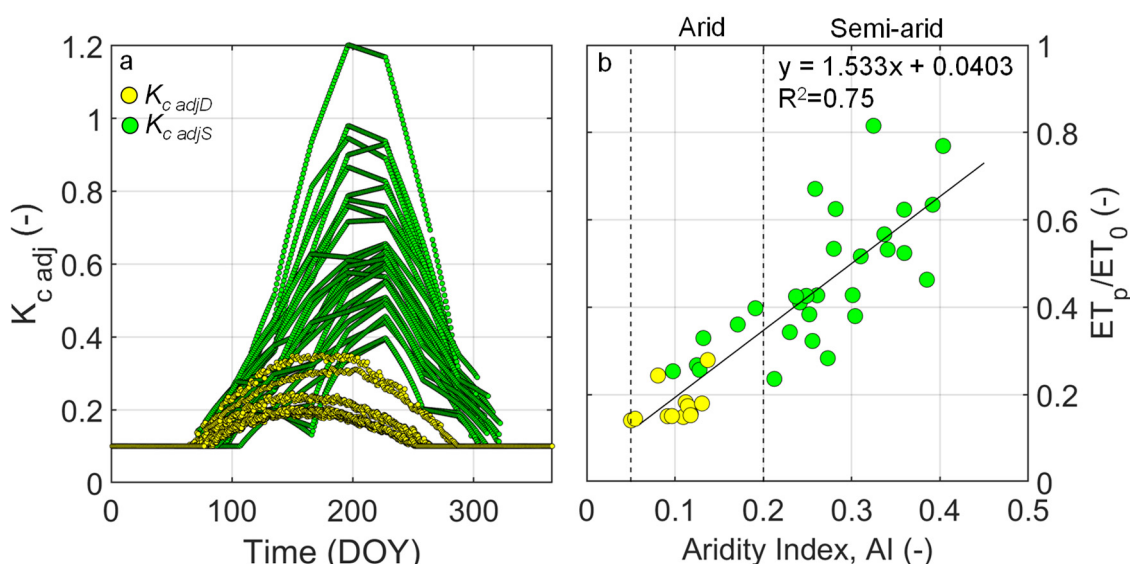


**Figure 10.** (a) daily  $K_{c\ adj}$  values (DOY depicts day of the year) and (b) relationship between aridity index,  $AI$ , and mean annual  $ET_p$  to  $ET_0$  ratio over 41 weather stations in Mongolia. Solid black line represents linear regression equation reported with associated  $R^2$ . Data are grouped according to natural vegetation zones, namely, steppe (green circles) and Gobi desert (yellow circles). Vertical dashed lines delimit climate classes (arid and semi-arid classes).

The relation between climate aridity (in terms of  $AI$ ) and the ratio of mean annual  $ET_p$  to mean annual  $ET_0$  (or  $ET_p/ET_0$ ) is shown in Figure 10b. Data are grouped according to the land cover class (Gobi Desert and steppe) and climate class (vertical dashed line delimits arid and semi-arid climate classes, respectively). The locations belonging to the Gobi Desert (yellow circles) cluster very closely in the arid class, while the steppe points are scattered mostly in the semi-arid climate. The fit of the linear regression shows an acceptable  $R^2$  value and describes more than 80% reduction of  $ET_0$  in the Gobi Desert and about 54% reduction in the steppe locations under semi-arid conditions.

#### 4. Discussion

The first goal of this study was to find a suitable temperature-based method to reliably estimate  $ET_0$  in Mongolia [6]. We compared the Hargreaves (Har) and Thornthwaite (Tho)



equations with the Penman–Monteith (FAO-56 PM) equation. The latter is highly recommended by the International Commission for Irrigation Drainage, Food and Agriculture Organization of the United Nations and ASCE-Evapotranspiration in Irrigation and Hydrology Committee [43,44]. Both Har-based and Tho-based models mostly underestimate FAO-56 PM-based average annual  $ET_0$  in most weather stations in arid and semi-arid conditions, as reported by previous studies [38,45]. The underestimation is observed in other studies evaluating the Har model in arid and semi-arid conditions in several parts of the world [46–49]. In this study, we propose to select the Har method, which outperforms the Tho equation to predict daily  $ET_0$ . A comparison between FAO-56 PM and Har equations for predicting  $ET_0$  has been carried out all over the world. Similar RMSE values between FAO-56 PM and the uncalibrated Har equation reported in Mongolia have also been observed in southern Italy [50], in south-east Spain [51], in the U.S. High Plains [39], and northwest China [52], while lower RMSE values are reported in arid and semi-arid areas in China [53]. The Har  $ET_0$  estimates can be considered acceptable as reported in some studies carried out in Mongolia [8,19,42].

The second goal of this study is the assessment of the biome-specific potential evapotranspiration,  $ET_p$ , in Mongolia. The key step is to find a suitable method to describe the crop coefficient,  $K_c$ , to convert  $ET_0$  into  $ET_p$ . The FAO-56 guidelines recommend the calculation of  $K_c$  in each crop growing phase. Larger-than-normal crop coefficient values should be attributed to a well-watered crop under arid and semi-arid climate conditions. It is expected that  $K_c$  should be larger under arid conditions when the agricultural crop has leaf area and roughness height greater than that of the reference grass. However, this is not the case in Mongolia.  $K_c$  values in Mongolia are currently unavailable in any type of natural vegetation. Very few studies have been conducted in semi-arid natural environments [13].

Even though two different methods were used to develop  $K_{c\ adj}$ -values depending on the biome ( $LAI$ -dependent  $K_{c\ adjS}$  in steppe,  $R_n$ -dependent  $K_{c\ adjD}$  in the Gobi Desert), the results have a smooth transition in  $K_{c\ adj}$ -values in the study locations. The  $K_{c\ adjD}$  estimates in the Gobi Desert region are similar to the results presented by [12,13] in Inner Mongolia. In well-managed cropland, the standard conditions are generally the actual field conditions. The  $ET_p$  is partitioned in potential evaporation and potential transpiration using available maps of  $LAI$  in Mongolia. The  $E_p$  constitutes a major part of  $ET_p$  with low  $LAI$  in the southern Gobi Desert locations, while  $T_p$  increases toward the northern region. According to [12,13], daily  $K_c$  values in the growing season ranged from 0.02 to 0.50 with an average value of 0.17 and 0.15 to 0.17 in a temperate desert in Inner Mongolia. Both studies were performed in the Gobi Desert (Inner Mongolia).

We observe that using tabulated  $K_c$  values in northern Mongolia is acceptable, while under sparse vegetation cover conditions (in central and southern Mongolia), we highly recommend to relate crop coefficient to easily-retrievable  $LAI$  (remote sensing maps) in the steppe region or to solar radiation in the Gobi Desert region. A proper prediction of  $ET_p$  is key to obtain successful model simulations. The impact of  $ET_p$  prediction on GR simulations will be treated in a follow-up study.

## 5. Conclusions

This study evaluates a protocol for estimating the  $ET_p$  in Mongolia under limited data availability. The majority of the auxiliary data required for this study have been collected from remote-sensing products and local ground-based measurements of meteorological data. This practice can be helpful under data paucity constraints in many areas with an arid/semi-arid climate.

It is necessary to reliably estimate  $ET_0$  based on temperature data in Mongolia. Despite some underestimation bias, we recommend the temperature-based Hargreaves equation that reliably predicts  $ET_0$ , as verified by comparison with FAO-56 PM results.

It is also necessary to assess the crop coefficient,  $K_c$ , to convert  $ET_0$  into  $ET_p$ . In this study, we introduce a modified time-variant crop coefficient,  $K_{c\ adj}$ , specific for the two main biomes in Mongolia, namely, the Gobi Desert ( $K_{c\ adjD}$ ) and the steppe grasslands ( $K_{c\ adjS}$ ).

The  $K_c$  values tabulated in the FAO guidelines generate spatially uniform predictions of  $ET_p$  over the 41 experimental locations characterized by contrasting vegetation cover. In contrast, the developed  $K_{c\ adj}$  value induces a drastic reduction in  $ET_p$  towards the arid zone. We, therefore, recommend using LAI-dependent  $K_{c\ adjS}$ -values in the steppe and radiation-dependent  $K_{c\ adjD}$ -values in the Gobi Desert zone. Approximately 80% and 54% reduction of  $ET_0$  into  $ET_p$  is reported in the Gobi Desert and in the steppe locations, respectively.

Model performance can be improved by increasing data availability and quality. On the one hand, the Hargreaves equation would benefit from long time series (in the order of decades) of air temperature to estimate  $ET_0$ . On the other hand, the empirical equations describing the adjusted crop coefficient values would be enhanced if based on direct measurements over representative hotspots in Gobi Desert and steppe biomes. Results can be used to develop  $K_{c\ adj}$  under natural vegetation conditions in similar areas. This methodology for predicting  $ET_p$  can be used in modeling tools of the vadose zone, climate models, and water balance studies with only a few parameters and without labor-demanding field measurements.

**Supplementary Materials:** The following are available online at <https://www.mdpi.com/article/10.3390/w13182470/s1>, Figure S1: Daily temperature (T) data retrieved from NAMEM (blue dots) and NOAA (red dots) at Khatgal weather station; Figure S2: Monthly mean LAI values in the growing season, extracted from the dataset by Mao and Yan (2019); Figure S3: Monthly mean LAI retrieved from ORNL DAAC over 41 study locations, Mongolia; Figure S4: Comparison between FAO-56 PM-based and temperature-based equations (Har  $ET_0$  values are represented by blue circles, and Tho  $ET_0$  values are depicted by red circles) for predicting daily values of  $ET_0$  at (a) Khatgal weather station, and (b) Tsogtovoov weather station; Figure S5: Comparison among three different methods (FAO-56 PM, Har, Tho) to predict monthly  $ET_0$  in 10 test locations, Mongolia; Figure S6: Geographical locations of six weather stations in the steppe region (Sukhbaatar, Tosontsengel, Baruunkharaa, Undurkhaan, Erdenesant, Arvaikheer) and one representative weather station in the Gobi Desert (Saikhanovoo); Figure S7: Mean monthly values of tabulated crop coefficient,  $K_c$  over six weather stations (Sukhbaatar, Tosontsengel, Baruunkharaa, Undurkhaan, Erdenesant, Arvaikheer) in the steppe zone (colored circles) and one weather station (Saikhanovoo) in the Gobi Desert (black square). Figure S8: Values of (a) mean annual temperature and (b) mean annual precipitation over the 41 weather stations (circles of varying size indicate variations in magnitude of the attribute) on digital elevation model (DEM) map from Earth Resources Observation And Science center, 2017 (SRTM); Figure S9: Mean annual values of  $ET_0$ ,  $ET_p$  and LAI over the 41 weather stations grouped in the Gobi Desert and steppe zones Figure S10: Mean annual values of  $ET_0$ ,  $ET_p$  and  $AI$  over the 41 weather stations grouped in the Gobi Desert and steppe zones.

**Author Contributions:** Conceptualization, K.B., V.A.Z., A.S. and P.N.; methodology, K.B., A.S., P.N. and V.A.Z.; software, K.B.; validation, P.N. and K.B.; formal analysis, K.B.; investigation, K.B.; resources, V.A.Z.; data curation, K.B. and P.N.; writing—original draft preparation, K.B., P.N. and V.A.Z.; writing—review and editing, K.B. and A.S.; visualization, P.N. and A.S.; supervision, V.A.Z., A.S. and P.N.; project administration, V.A.Z.; funding acquisition, V.A.Z. All authors have read and agreed to the published version of the manuscript.

**Funding:** This study was supported by the Fulbright scholarship from 2019 to 2021 to Khulan Batsukh and grant to Vitaly Zlotnik from Daugherty Water for Food Institute, University of Nebraska.

**Institutional Review Board Statement:** Not applicable.

**Informed Consent Statement:** Not applicable.

**Data Availability Statement:** Not applicable.

**Acknowledgments:** We are grateful to the National Agency for Meteorology and Environmental Monitoring (NAMEM), Mongolia, and Jadambaa Namjil (Institute of Geography and Geoecology), Gomboluudev Purevjav (Institute of Meteorology and Hydrology), and Ariunaa Chinbat (Mongolian Association of Hydrogeologists) for sharing data.

**Conflicts of Interest:** The authors declare no conflict of interest.

## Appendix A

**Table A1.** Categorization of natural zones.

ID.	Stations	Natural Zone	ID.	Stations	Natural Zone
1	Sukhbaatar	Steppe	22	Baynuul	steppe
2	Tseterleg	Steppe	23	Galuut	steppe
3	Bulgan Mg	Steppe	24	Ulaangom	steppe
4	Khatgal	Steppe	25	Arvaikheer	steppe
5	Tosontsengel	Steppe	26	Choir	steppe
6	Binder	Steppe	27	Mandalgobi	steppe
7	Rinchinlhumbe	Steppe	28	Altai	steppe
8	Khalkh gol	Steppe	29	Khoriult	steppe
9	Erdenemandal	Steppe	30	Hovd	Gobi Desert
10	Baruunkharaa	Steppe	31	Ulgii	Gobi Desert
11	Baruunturuun	Steppe	32	Ekhiingol	Gobi Desert
12	Erdenetsagaan	Steppe	33	Gurvantes	Gobi Desert
13	Chingis khaan (UB)	Steppe	34	Tooroi	Gobi Desert
14	Choibalsan	Steppe	35	Sainshand	Gobi Desert
15	Undurkhaan	Steppe	36	Khanbogd	Gobi Desert
16	Matad	Steppe	37	Zamiin Uud	Gobi Desert
17	Murun	Steppe	38	Baitag	Gobi Desert
18	Uliastai	Steppe	39	Dalanzadgad	Gobi Desert
19	Baruun-Urt	Steppe	40	Saikhan-Ovoo	Gobi Desert
20	Erdenesant	Steppe	41	Tsogt-Ovoo	Gobi Desert
21	Dariganga	Steppe			

**Table A2.** Annual sums of  $ET_0$  over the 41 weather stations in Mongolia.

ID.	Stations	Annual Har $ET_0$ (mm)					Mean Har $ET_0$ (mm)	CV (%)
		2007	2008	2009	2010	2011		
1	Sukhbaatar	861	847	929	812	812	852	5.6
2	Tseterleg	845	819	801	763	769	799	4.3
3	Bulgan Mg	891	854	854	835	782	843	4.7
4	Khatgal	742	715	694	691	695	707	3
5	Tosontsengel	791	762	753	696	729	746	4.8
6	Binder	907	818	823	793	840	836	5.1
7	Rinchinlhumbe	723	686	663	666	687	685	3.5
8	Khalkh gol	910	872	834	863	839	863	3.5
9	Erdenemandal	871	836	810	793	789	820	4.2
10	Baruunkharaa	921	889	884	846	849	878	3.5
11	Baruunturuun	792	769	727	713	749	750	4.2
12	Erdenetsagaan	926	848	847	849	820	858	4.7
13	Chingis khaan (UB)	584	561	571	757	694	634	13.8
14	Choibalsan	952	881	876	860	880	890	4
15	Undurkhaan	987	914	883	874	894	910	5
16	Matad	976	882	882	877	854	894	5.3
17	Murun	865	834	814	777	798	817	4.1

Table A2. Cont.

ID.	Stations	Annual Har $ET_0$ (mm)					Mean Har $ET_0$ (mm)	CV (%)
		2007	2008	2009	2010	2011		
18	Uliastai	842	818	790	755	772	795	4.4
19	Baruun-Urt	972	896	900	880	862	902	4.6
20	Erdenesant	881	843	804	772	750	810	6.5
21	Dariganga	835	841	819	864	866	845	2.4
22	Baynuul	819	770	741	714	735	756	5.4
23	Galuut	769	797	763	739	708	755	4.4
24	Ulaangom	863	846	798	790	819	823	3.8
25	Arvaikheer	830	808	825	780	776	804	3.1
26	Choir	954	893	898	857	839	888	5
27	MandalGobi	954	915	922	861	871	905	4.2
28	Altai	778	753	740	691	706	733	4.8
29	Khoriult	987	982	1001	955	952	975	2.2
30	Hovd	902	898	867	824	846	867	3.9
31	Ulgii	846	838	781	777	808	810	3.9
32	Ekhiingol	1121	1139	1159	1106	1118	1129	1.8
33	Gurvantes	886	891	921	869	871	888	2.4
34	Tooroi	1104	1130	1121	1039	1038	1086	4.1
35	Sainshand	1029	1000	1012	984	952	996	2.9
36	Khanbogd	1034	995	1029	971	983	1002	2.8
37	Zamiin Uud	1033	1010	1041	1002	1010	1019	1.7
38	Baitag	1000	1006	957	886	964	962	5
39	Dalanzadgad	985	985	1012	964	960	981	2.1
40	Saikhan-Ovoo	981	957	1003	946	926	963	3.1
41	Tsogt-Ovoo	1015	985	1012	955	936	981	3.5
Spatial-average $ET_0$		902	873	867	840	843		

Table A3. Mean annual sums of water fluxes over 41 weather stations in Mongolia.

ID.	Stations	$P$ (mm)	$ET_0$ (mm)	$ET_p$ (mm)	$E_p$ (mm)	$T_p$ (mm)	$AI$	Class
1	Sukhbaatar	277	852	695	329	366	0.32	Semi-arid
2	Tseterleg	323	799	615	270	344	0.4	Semi-arid
3	Bulgan Mg	287	843	448	284	164	0.34	Semi-arid
4	Khatgal	277	707	449	245	204	0.39	Semi-arid
5	Tosontsengel	193	746	501	271	230	0.26	Semi-arid
6	Binder	301	836	521	297	224	0.36	Semi-arid
7	Rinchinlumbe	193	685	428	243	185	0.28	Semi-arid
8	Khalkh gol	291	863	489	299	190	0.34	Semi-arid
9	Erdenemandal	254	820	423	269	154	0.31	Semi-arid
10	Baruunkharaa	316	878	460	298	162	0.36	Semi-arid
11	Baruunturuun	210	750	400	266	135	0.28	Semi-arid
12	Erdenetsagaan	207	858	353	233	120	0.24	Semi-arid
13	Chingis khaan (UB)	244	634	293	207	86	0.39	Semi-arid
14	Choibalsan	205	890	305	197	108	0.23	Semi-arid
15	Undurkhaan	238	910	389	291	98	0.26	Semi-arid
16	Matad	211	849	362	267	95	0.25	Semi-arid
17	Murun	227	755	323	232	90	0.3	Semi-arid
18	Uliastai	188	795	338	247	91	0.24	Semi-arid
19	Baruun-Urt	172	902	359	270	88	0.19	Arid
20	Erdenesant	246	810	308	237	71	0.3	Semi-arid
21	Dariganga	145	845	305	239	66	0.17	Arid
22	Baynuul	190	756	290	225	65	0.25	Semi-arid
23	Galuut	193	755	244	196	47	0.26	Semi-arid
24	Ulaangom	109	823	271	223	48	0.13	Arid
25	Arvaikheer	219	804	228	187	41	0.27	Semi-arid

Table A3. Cont.

ID.	Stations	P (mm)	ET <sub>0</sub> (mm)	ET <sub>p</sub> (mm)	E <sub>p</sub> (mm)	T <sub>p</sub> (mm)	AI	Class
26	Choir	111	888	237	200	38	0.12	Arid
27	MandalGobi	93	731	188	161	26	0.13	Arid
28	Altai	156	733	173	150	23	0.21	Semi-arid
29	Khoriult	95	975	247	212	35	0.1	Arid
30	Khovd	119	867	242	210	32	0.14	Arid
31	Ulgii	95	810	126	108	18	0.12	Arid
32	Ekhiingol	57	1129	159	139	20	0.05	Arid
33	Gurvantes	100	888	162	141	21	0.11	Arid
34	Tooroi	60	1086	157	137	21	0.05	Arid
35	Sainshand	109	996	148	133	16	0.11	Arid
36	Khanbogd	115	1002	174	156	18	0.11	Arid
37	Zamiin Uud	93	1019	154	138	16	0.09	Arid
38	Baitag	93	962	145	131	14	0.1	Arid
39	Dalanzadgad	128	981	176	161	15	0.13	Arid
40	Saikhan-Ovoo	113	963	147	134	13	0.12	Arid
41	Tsogt-Ovoo	79	981	239	218	21	0.08	Arid

## References

- Ma, X.; Yasunari, T.; Ohata, T.; Natsagdorj, L.; Davaa, G.; Oyunbaatar, D. Hydrological regime analysis of the Selenge River basin, Mongolia. *Hydrol. Process.* **2003**, *17*, 2929–2945. [\[CrossRef\]](#)
- Allen, R.G.; Pereira, L.S.; Raes, D.; Smith, M. Crop evapotranspiration: Guidelines for Computing Crop Water Requirements. *Food Agric. Organ. USA* **1998**, *300*, D05109.
- Šimůnek, J.; van Genuchten, M.T.; Šejna, M. Recent Developments and Applications of the HYDRUS Computer Software Packages. *Vadose Zo. J.* **2016**, *15*, vzj2016.04.0033. [\[CrossRef\]](#)
- Beegum, S.; Šimůnek, J.; Szymkiewicz, A.; Sudheer, K.P.; Nambi, I.M. Updating the Coupling Algorithm between HYDRUS and MODFLOW in the HYDRUS Package for MODFLOW. *Vadose Zo. J.* **2018**, *17*, 180034. [\[CrossRef\]](#)
- Srivastava, A.; Sahoo, B.; Raghuwanshi, N.S.; Singh, R. Evaluation of Variable-Infiltration Capacity Model and MODIS-Terra Satellite-Derived Grid-Scale Evapotranspiration Estimates in a River Basin with Tropical Monsoon-Type Climatology. *J. Irrig. Drain. Eng.* **2017**, *143*, 04017028. [\[CrossRef\]](#)
- Sahoo, B.; Walling, I.; Deka, B.C.; Bhatt, B.P. Standardization of Reference Evapotranspiration Models for a Subhumid Valley Rangeland in the Eastern Himalayas. *J. Irrig. Drain. Eng.* **2012**, *138*, 880–895. [\[CrossRef\]](#)
- Adamala, S.; Raghuwanshi, N.S.; Mishra, A.K.; Tiwari, M.K. Evapotranspiration Modeling Using Second-Order Neural Networks. *J. Hydrol. Eng.* **2014**, *19*, 1131–1140. [\[CrossRef\]](#)
- Yu, W.; Wu, T.; Wang, W.; Li, R.; Wang, T.; Qin, Y.; Wang, W.; Zhu, X. Spatiotemporal Changes of Reference Evapotranspiration in Mongolia during 1980–2006. *Adv. Meteorol.* **2016**, *2016*, 9586896. [\[CrossRef\]](#)
- Xiang, K.; Li, Y.; Horton, R.; Feng, H. Similarity and difference of potential evapotranspiration and reference crop evapotranspiration—A review. *Agric. Water Manag.* **2020**, *232*, 106043. [\[CrossRef\]](#)
- McMahon, T.A.; Peel, M.C.; Lowe, L.; Srikanthan, R.; McVicar, T.R. Estimating actual, potential, reference crop and pan evaporation using standard meteorological data: A pragmatic synthesis. *Hydrol. Earth Syst. Sci.* **2013**, *17*, 1331–1363. [\[CrossRef\]](#)
- Nandintsetseg, B.; Shinoda, M. Seasonal change of soil moisture in Mongolia: Its climatology and modelling. *Int. J. Clim.* **2010**, *31*, 1143–1152. [\[CrossRef\]](#)
- Yang, F.; Zhou, G. Characteristics and modeling of evapotranspiration over a temperate desert steppe in Inner Mongolia, China. *J. Hydrol.* **2011**, *396*, 139–147. [\[CrossRef\]](#)
- Zhang, F.; Zhou, G.; Wang, Y.; Yang, F.; Nilsson, C. Evapotranspiration and crop coefficient for a temperate desert steppe ecosystem using eddy covariance in Inner Mongolia, China. *Hydrol. Process.* **2011**, *26*, 379–386. [\[CrossRef\]](#)
- Ren, X.; Qu, Z.; Martins, D.S.; Paredes, P.; Pereira, L.S. Daily Reference Evapotranspiration for Hyper-Arid to Moist Sub-Humid Climates in Inner Mongolia, China: I. Assessing Temperature Methods and Spatial Variability. *Water Resour. Manag.* **2016**, *30*, 3769–3791. [\[CrossRef\]](#)
- Xia, J.; Liang, S.; Chen, J.; Yuan, W.; Liu, S.; Li, L.; Cai, W.; Zhang, L.; Fu, Y.; Zhao, T.; et al. Satellite-Based Analysis of Evapotranspiration and Water Balance in the Grassland Ecosystems of Dryland East Asia. *PLoS ONE* **2014**, *9*, e97295. [\[CrossRef\]](#)
- Lamchin, M.; Park, T.; Lee, J.-Y.; Lee, W.-K. Monitoring of Vegetation Dynamics in the Mongolia Using MODIS NDVIs and their Relationship to Rainfall by Natural Zone. *J. Indian Soc. Remote Sens.* **2014**, *43*, 325–337. [\[CrossRef\]](#)
- Yembuu, B. *General Geographical Characteristics of Mongolia BT—The Physical Geography of Mongolia*; Yembuu, B., Ed.; Springer: Cham, Switzerland, 2021; pp. 1–8.
- Indree, T. *The Steppe Vegetation of Mongolia*; Bembi San: Ulaanbaatar, Mongolia, 2014.
- Li, S.-G.; Asanuma, J.; Kotani, A.; Davaa, G.; Oyunbaatar, D. Evapotranspiration from a Mongolian steppe under grazing and its environmental constraints. *J. Hydrol.* **2007**, *333*, 133–143. [\[CrossRef\]](#)



20. Earth Resources Observation And Science Center. *Shuttle Radar Topography Mission (SRTM) 3 Arc-Second Global*; Earth Resources Observation And Science Center: Sioux Falls, SD, USA, 2017.
21. National Agency for Meteorology and Environmental Monitoring, Precipitation. Available online: <http://tsag-agaar.gov.mn/> (accessed on 27 May 2020).
22. Menne, M.J.; Durre, I.; Korzeniewski, B.; McNeill, S.; Thomas, X.; Yin, K. *Global Historical Climatology Network—Daily (GHCN-Daily)*; Version 3; NOAA National Centers for Environmental Information: Asheville, NC, USA, 2012. Available online: <https://www.ncdc.noaa.gov/cdo-web/> (accessed on 27 May 2020).
23. Mao, J.; Yan, B. *Global Monthly Mean Leaf Area Index Climatology, 1981–2015*; ORNL DAAC: Oak Ridge, TN, USA, 2019.
24. Lama, G.F.C.; Errico, A.; Francalanci, S.; Solari, L.; Preti, F.; Chirico, G.B. Evaluation of Flow Resistance Models Based on Field Experiments in a Partly Vegetated Reclamation Channel. *Geosciences* **2020**, *10*, 47. [\[CrossRef\]](#)
25. Hargreaves, G.H.; Samani, Z.A. Reference Crop Evapotranspiration from Temperature. *Appl. Eng. Agric.* **1985**, *1*, 96–99. [\[CrossRef\]](#)
26. Thornthwaite, C.W. An Approach toward a Rational Classification of Climate. *Geogr. Rev.* **1948**, *38*, 55–94. [\[CrossRef\]](#)
27. Mintz, Y.; Walker, G.K. Global Fields of Soil Moisture and Land Surface Evapotranspiration Derived from Observed Precipitation and Surface Air Temperature. *J. Appl. Meteorol.* **1993**, *32*, 1305–1334. [\[CrossRef\]](#)
28. Peng, L.; Li, Y.; Feng, H. The best alternative for estimating reference crop evapotranspiration in different sub-regions of mainland China. *Sci. Rep.* **2017**, *7*, 5458. [\[CrossRef\]](#)
29. Paredes, P.; Pereira, L.; Almorox, J.; Darouich, H. Reference grass evapotranspiration with reduced data sets: Parameterization of the FAO Penman-Monteith temperature approach and the Hargreaves-Samani equation using local climatic variables. *Agric. Water Manag.* **2020**, *240*, 106210. [\[CrossRef\]](#)
30. Srivastava, A.; Sahoo, B.; Raghuwanshi, N.S.; Chatterjee, C. Modelling the dynamics of evapotranspiration using Variable Infiltration Capacity model and regionally calibrated Hargreaves approach. *Irrig. Sci.* **2018**, *36*, 289–300. [\[CrossRef\]](#)
31. WeatherOnline Ltd. Weather Online Website. 2021. Available online: <https://www.weatheronline.co.uk/weather/maps/forecastmaps?LANG=en&CONT=asia&ION=0026&LAND=VM&UP=1&R=0&CEL=C> (accessed on 10 October 2020).
32. Spinoni, J.; Vogt, J.; Naumann, G.; Carrao, H.; Barbosa, P. Towards identifying areas at climatological risk of desertification using the Köppen-Geiger classification and FAO aridity index. *Int. J. Clim.* **2014**, *35*, 2210–2222. [\[CrossRef\]](#)
33. Sumner, D.M.; Jacobs, J.M. Utility of Penman–Monteith, Priestley–Taylor, reference evapotranspiration, and pan evaporation methods to estimate pasture evapotranspiration. *J. Hydrol.* **2005**, *308*, 81–104. [\[CrossRef\]](#)
34. Ritchie, J.T. Model for predicting evaporation from a row crop with incomplete cover. *Water Resour. Res.* **1972**, *8*, 1204–1213. [\[CrossRef\]](#)
35. Nasta, P.; Gates, J.B. Plot-scale modeling of soil water dynamics and impacts of drought conditions beneath rainfed maize in Eastern Nebraska. *Agric. Water Manag.* **2013**, *128*, 120–130. [\[CrossRef\]](#)
36. Adane, Z.; Zlotnik, V.A.; Rossman, N.R.; Wang, T.; Nasta, P. Sensitivity of Potential Groundwater Recharge to Projected Climate Change Scenarios: A Site-Specific Study in the Nebraska Sand Hills, USA. *Water* **2019**, *11*, 950. [\[CrossRef\]](#)
37. Wang, K.; Wang, P.; Li, Z.; Cribb, M.; Sparrow, M. A simple method to estimate actual evapotranspiration from a combination of net radiation, vegetation index, and temperature. *J. Geophys. Res. Atmos.* **2007**, *112*, D15107. [\[CrossRef\]](#)
38. Bian, Y.; Dai, H.; Zhang, Q.; Yang, L.; Du, W. Spatial distribution of potential evapotranspiration trends in the Inner Mongolia Autonomous Region (1971–2016). *Theor. Appl. Clim.* **2020**, *140*, 1161–1169. [\[CrossRef\]](#)
39. Kukal, M.S.; Irmak, S.; Walia, H.; Odhiambo, L. Spatio-temporal calibration of Hargreaves-Samani model to estimate reference evapotranspiration across U.S. High Plains. *Agron. J.* **2020**, *112*, 4232–4248. [\[CrossRef\]](#)
40. Song, X.; Lu, F.; Xiao, W.; Zhu, K.; Zhou, Y.; Xie, Z. Performance of 12 reference evapotranspiration estimation methods compared with the Penman-Monteith method and the potential influences in northeast China. *Meteorol. Appl.* **2018**, *26*, 83–96. [\[CrossRef\]](#)
41. FAO. *Global Map of Yearly Crop Reference Evapotranspiration*; FAO: Rome, Italy, 2009.
42. Zorigt, M.; van der Linden, W.; Garamaa, D. *Part 2. Integrated Water Management—National Assessment Report Volume I; IWRM*: Ulaanbaatar, Mongolia, 2012.
43. Allen, R.G.; Smith, M.; Pereira, L.S.; Perrier, A. An update for the calculation of reference evapotranspiration. *ICID Bull.* **1994**, *43*, 35–92.
44. Walter, I.A. *The ASCE Standardized Reference Evapotranspiration Equation*; Water Resour. Institute; ASCE: Reston, VA, USA, 2004.
45. Weiß, M.; Menzel, L. A global comparison of four potential evapotranspiration equations and their relevance to stream flow modelling in semi-arid environments. *Adv. Geosci.* **2008**, *18*, 15–23. [\[CrossRef\]](#)
46. Amatya, D.M.; Skaggs, R.W.; Gregory, J.D. Comparison of Methods for Estimating REF-ET. *J. Irrig. Drain. Eng.* **1995**, *121*, 427–435. [\[CrossRef\]](#)
47. Xu, C.-Y.; Singh, V.P. Cross Comparison of Empirical Equations for Calculating Potential Evapotranspiration with Data from Switzerland. *Water Resour. Manag.* **2002**, *16*, 197–219. [\[CrossRef\]](#)
48. Tabari, H.; Talaei, P.H. Local Calibration of the Hargreaves and Priestley-Taylor Equations for Estimating Reference Evapotranspiration in Arid and Cold Climates of Iran Based on the Penman-Monteith Model. *J. Hydrol. Eng.* **2011**, *16*, 837–845. [\[CrossRef\]](#)
49. Mohawesh, O.E.; Taloezi, S.A. Comparison of Hargreaves and FAO56 equations for estimating monthly evapotranspiration for semi-arid and arid environments. *Arch. Agron. Soil Sci.* **2012**, *58*, 321–334. [\[CrossRef\]](#)

- 
50. Pelosi, A.; Medina, H.; Villani, P.; D'Urso, G.; Chirico, G. Probabilistic forecasting of reference evapotranspiration with a limited area ensemble prediction system. *Agric. Water Manag.* **2016**, *178*, 106–118. [[CrossRef](#)]
  51. Gomariz-Castillo, F.; Alonso-Sarriá, F.; Cabezas-Calvo-Rubio, F. Calibration and spatial modelling of daily ET0 in semiarid areas using Hargreaves equation. *Earth Sci. Inform.* **2017**, *11*, 325–340. [[CrossRef](#)]
  52. Celestin, S.; Qi, F.; Li, R.; Yu, T.; Cheng, W. Evaluation of 32 Simple Equations against the Penman–Monteith Method to Estimate the Reference Evapotranspiration in the Hexi Corridor, Northwest China. *Water* **2020**, *12*, 2772. [[CrossRef](#)]
  53. Gao, F. Evaluation of Reference Evapotranspiration Methods in Arid, Semiarid, and Humid Regions. *J. Am. Water Resour. Assoc.* **2017**, *53*, 791–808. [[CrossRef](#)]